J|A|C|S ARTICLES

Published on Web 05/26/2009

Metal-Ion Mutagenesis: Conversion of a Purple Acid Phosphatase from Sweet Potato to a Neutral Phosphatase with the Formation of an Unprecedented Catalytically Competent $Mn^{II}Mn^{II}$ Active Site

Nataša Mitić,[†] Christopher J. Noble,[‡] Lawrence R. Gahan,[†] Graeme R. Hanson,*[,‡] and Gerhard Schenk*[,†]

School of Chemistry and Molecular Biosciences, and Centre of Magnetic Resonance, The University of Queensland, Queensland, Australia, 4072

Received February 1, 2009; E-mail: graeme.hanson@cmr.uq.edu.au; schenk@uq.edu.au

Abstract: The currently accepted paradigm is that the purple acid phosphatases (PAPs) require a heterovalent, dinuclear metal-ion center for catalysis. It is believed that this is an essential feature for these enzymes in order for them to operate under acidic conditions. A PAP from sweet potato is unusual in that it appears to have a specific requirement for manganese, forming a unique Fe^{III}-μ-(O)-Mn^{II} center under catalytically optimal conditions (Schenk et al. *Proc. Natl. Acad. Sci. U.S.A.* **2005**, *102*, 273). Herein, we demonstrate, with detailed electron paramagnetic resonance (EPR) spectroscopic and kinetic studies, that in this enzyme the chromophoric Fe^{III} can be replaced by Mn^{II}, forming a catalytically active, unprecedented antiferromagnetically coupled homodivalent Mn^{II}-μ-(H)OH-μ-carboxylato-Mn^{II} center in a PAP. However, although the enzyme is still active, it no longer functions as an acid phosphatase, having optimal activity at neutral pH. Thus, PAPs may have evolved from distantly related divalent dinuclear metallohydrolases that operate under pH neutral conditions by stabilization of a trivalent−divalent metal-ion core. The present Mn^{II}−Mn^{II} system models these distant relatives, and the results herein make a significant contribution to our understanding of the role of the chromophoric metal ion as an activator of the nucleophile. In addition, the detailed analysis of strain broadened EPR spectra from exchange-coupled dinuclear Mn^{II}−Mn^{II} centers described herein provides the basis for the full interpretation of the EPR spectra from other dinuclear Mn metalloenzymes.

Introduction

Purple acid phosphatases (PAPs) belong to the family of dinuclear metallohydrolases that include Ser/Thr protein phosphatases, organophosphate-degrading triesterases, ureases, arginases, aminopeptidases, and antibiotics-degrading metallo-β-lactamases.[1−6] Because of their widespread metabolic functions, several of these enzymes have become targets for the development of chemotherapeutic agents or are used as bioremediators. Specifically, PAP activity in animals has been shown to be directly linked to bone resorption; overexpression of this enzyme by bone-resorbing osteoclasts leads to osteoporosis.[7,8] Consequently, PAP has become a major target in the development of anti-osteoporotic drugs.[9]

Virtually all dinuclear metallohydrolases have homodivalent metal centers of the $Zn^{II}Zn^{II}$, $Fe^{II}Fe^{II}$, or $Mn^{II}Mn^{II}$ type.[1,6] The only exception with a confirmed heterodivalent dinuclear center of the type $Fe^{III}M^{II}$ (M = Fe, Zn, Mn) is PAP.[1,6,10,11] Despite a low degree of overall amino acid sequence homology and metal-ion content between enzymes from different kingdoms[12] their catalytic sites display a remarkable similarity. The two metal ions are coordinated by seven invariant ligands (Figure 1), with an aspartate residue bridging the two ions.[13] The characteristic purple color of PAPs is due to the formation of a charge-transfer (CT) complex between the trivalent iron and a conserved tyrosine ligand.[14] Animal PAPs have a redox-active

[†] School of Chemistry and Molecular Biosciences.
[‡] Centre of Magnetic Resonance.

(1) Wilcox, D. E. *Chem. Rev.* **1996**, *96*, 2435–2458.
(2) Dismukes, G. C. *Chem. Rev.* **1996**, *96*, 2909–2926.
(3) Barford, D.; Das, A. K.; Egloff, M. P. *Annu. Rev. Biophys. Biomol. Struct.* **1998**, *27*, 133–164.
(4) Lowther, W. T.; Matthews, B. W. *Biochim. Biophys. Acta* **2000**, *1477*, 157–167.
(5) Crowder, M. W.; Spencer, J.; Vila, A. J. *Acc. Chem. Res.* **2006**, *39*, 721–728.
(6) Mitić, N.; Smith, S. J.; Neves, A.; Guddat, L. W.; Gahan, L. R.; Schenk, G. *Chem. Rev.* **2006**, *106*, 3338–3363.
(7) Hayman, A. R.; Jones, S. J.; Boyde, A.; Foster, D.; Colledge, W. H.; Carlton, M. B.; Cox, T. M. *Development* **1996**, *122*, 3151–3162.
(8) Oddie, G. W.; Schenk, G.; Angel, N. Z.; Walsh, N.; Guddat, L. W.; de Jersey, J.; Cassady, A. I.; Hamilton, S. E.; Hume, D. A. *Bone* **2000**, *27*, 575–584.
(9) (a) Valizadeh, M.; Schenk, G.; Nash, K.; Oddie, G. W.; Guddat, L. W.; Hume, D. A.; de Jersey, J.; Burke, T. R.; Hamilton, S. *Arch. Biochem. Biophys.* **2004**, *424*, 154–162. (b) McGeary, R. P.; Vella, P.; Mak, J. Y. W.; Guddat, L. W.; Schenk, G. *Bioorg. Med. Chem. Lett.* **2009**, *19*, 163–166.
(10) Wang, D. L.; Holz, R. C.; David, S. S.; Que Jr, L.; Stankovich, M. T. *Biochemistry* **1991**, *30*, 8187–8194.
(11) Bernhardt, P. V.; Schenk, G.; Wilson, G. V. *Biochemistry* **2004**, *43*, 10387–10392.
(12) (a) Schenk, G.; Guddat, L. W.; Ge, Y.; Carrington, L. E.; Hume, D. A.; Hamilton, S.; de Jersey, J. *Gene* **2000**, *250*, 117–125. (b) Flanagan, J. U.; Cassady, A. I.; Schenk, G.; Guddat, L. W.; Hume, D. A. *Gene* **2006**, *377*, 12–20.

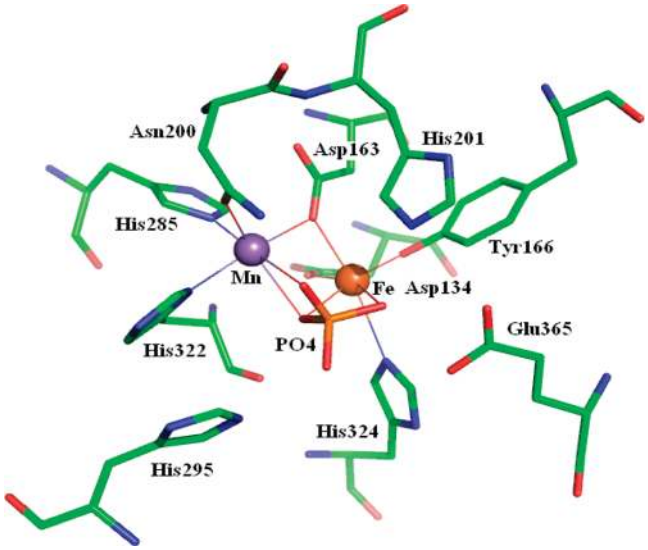

Figure 1. Schematic illustration of the active site of FeMn-spPAP.[13e] His201, His295, and Glu365 assist in substrate binding and orientation. The substrate analogue (PO_4) is shown in a possible transition state whereby the bridging oxygen acts as a nucleophile.

$Fe^{III}Fe^{III/II}$ center, where only the mixed-valent form is believed to be catalytically competent.[15] Reduction of the active $Fe^{III}Fe^{II}$ center to $Fe^{II}Fe^{II}$ leads to inactivation and loss of one or both metal ions depending upon exposure times to the reductant.[16,17] In fact, this approach has been successfully employed to generate metalloderivatives of PAPs.[16−23] For instance, the Fe^{II} in pig PAP (uteroferrin) can be replaced by Zn^{II} without a significant change in activity, whereas the Mn^{II}, Ni^{II}, Cu^{II}, and Co^{II} derivatives display 10−50% activity of the native enzyme.[19,21−23] Although the divalent ion can be replaced, there are no reports of catalytically active dinuclear homodivalent PAPs. In most plant PAPs the divalent metal ion (M^{II}) is either Zn^{II} or Mn^{II}.[24−26] The precise mechanistic role(s) of the two metal ions is still subject to debate, but it has been proposed that the M^{II} is essential in substrate binding and orientation and the Fe^{III} activates the hydrolysis-initiating nucleophile.[27−31] Herein, we have probed the role of the Fe^{III} by substituting it with manganese. We chose a PAP from sweet potato (spPAP) as the target enzyme because it has previously been shown to require at least one Mn in the active site, forming an unprecedented, strongly antiferromagnetically coupled Fe^{III}-(μ-O)-Mn^{II} center under optimal catalytic conditions (Figure 1).[13e,32]

Experimental Section

Protein Purification and Metal-Ion Replacement. spPAP was purified as described previously.[25] To generate the Mn derivative, the native FeMn enzyme (0.3 mM in 0.1 M acetate buffer, pH 4.9) was incubated at room temperature (RT) with 5 mM 1,10-phenanthroline and 100 mM sodium dithionite for 20 min. The mixture was loaded onto a 3 mL Bio-Rad Econo-Pac 10DG column (equilibrated with 0.1 M acetate buffer, pH 4.9). Subsequently, 50 equiv of $MnCl_2$ was added and the mixture was allowed to stand at RT for several days until maximal kinetic activity was reached (~100 h). The excess of manganese was then removed by dialysis against 0.1 M acetate buffer, pH 4.9. The metal-ion composition was determined in triplicate using atomic absorption spectroscopy (Varian SpectrAA 220FS instrument).

Kinetics. The rates of product formation were determined at 25 °C using a standard continuous assay with *para*-nitrophenylphosphate (*p*-NPP) as substrate (λ = 390 nm; the $\Delta\varepsilon$ was determined at each pH by allowing 5 mM *p*-NPP to hydrolyze to completion). Measurements were carried out at various pH values ranging from pH 3.5 to pH 9.0 (using 0.1 M glycine, acetate, 2-(*N*-morpholino)-ethanesulfonic acid, and tris(hydroxymethyl)aminomethane buffers, respectively, each with 0.2 M KCl) using a Cary 50 Bio Spectrophotometer. Substrate concentrations ranged from 0.25 to 10 mM, and [PAP] was 2 nM. The pH dependence of the k_{cat} and k_{cat}/K_M values were fitted to eqs 1 and 2 as described elsewhere.[22,33]

$$k_{cat} = k_{cat1} + \left(\left\{(k_{cat4} - k_{cat1})K_{es1}K_{es2}K_{es3} + (k_{cat3} - k_{cat1})K_{es1}K_{es2}[H^+] + (k_{cat2} - k_{cat1})K_{es1}[H^+]^2\right\}/\left\{[H^+]^3 + K_{es1}[H^+]^2 + K_{es1}K_{es2}[H^+] + K_{es1}K_{es2}K_{es3}\right\}\right) \quad (1)$$

where K_{esn} (n = 1, 2, 3) represents a protonation equilibrium of the enzyme−substrate complex and k_{catn} (n = 1, 2, 3, 4) corresponds to the activity of the associated protonation states.

(13) (a) Sträter, N.; Klabunde, T.; Tucker, P.; Witzel, H.; Krebs, B. *Science* **1995**, *268*, 1489–1492. (b) Klabunde, T.; Sträter, N.; Frohlich, R.; Witzel, H.; Krebs, B. *J. Mol. Biol.* **1996**, *259*, 737–748. (c) Lindqvist, Y.; Johansson, E.; Kaija, H.; Vihko, P.; Schneider, G. *J. Mol. Biol.* **1999**, *291*, 135–147. (d) Uppenberg, J.; Lindqvist, F.; Svensson, C.; Ek-Rylander, B.; Andersson, G. *J. Mol. Biol.* **1999**, *290*, 201–211. (e) Schenk, G.; Gahan, L. R.; Carrington, L. E.; Mitić, N.; Valizadeh, M.; Hamilton, S. E.; de Jersey, J.; Guddat, L. W. *Proc. Natl. Acad. Sci. U.S.A.* **2005**, *102*, 273–278. (f) Sträter, N.; Jasper, B.; Scholte, M.; Krebs, B.; Duff, A. P.; Langley, D. B.; Han, R. L.; Averill, B. A.; Freeman, H. C.; Guss, J. M. *J. Mol. Biol.* **2005**, *351*, 233–246. (g) Guddat, L. W.; McAlpine, A. S.; Hume, D.; Hamilton, S.; de Jersey, J.; Martin, J. L. *Structure* **1999**, *7*, 757–767.
(14) Yang, Y. S.; McCormick, J. M.; Solomon, E. I. *J. Am. Chem. Soc.* **1997**, *119*, 11832–11842.
(15) Merkx, M.; Averill, B. A. *Biochemistry* **1998**, *37*, 8490–8497.
(16) Beck, J. L.; Keough, D. T.; deJersey, J.; Zerner, B. *Biochim. Biophys. Acta* **1984**, *791*, 357–363.
(17) Keough, D. T.; Dionysius, D. A.; deJersey, J.; Zerner, B. *Biochem. Biophys. Res. Commun.* **1980**, *94*, 600–605.
(18) Davis, J. C.; Averill, B. A. *Proc. Natl. Acad. Sci. U.S.A.* **1982**, *79*, 4623–4627.
(19) Beck, J. L.; McArthur, M. J.; deJersey, J.; Zerner, B. *Inorg. Chim. Acta* **1998**, *153*, 39–44.
(20) Merkx, M.; Averill, B. A. *J. Am. Chem. Soc.* **1999**, *121*, 6683–6689.
(21) Twitchett, M. B.; Schenk, G.; Aquino, M. A. S.; Yui, D. T. Y.; Lau, T. C.; Sykes, A. G. *Inorg. Chem.* **2002**, *41*, 5787–5794.
(22) Smith, S. J.; Casellato, A.; Hadler, K. S.; Mitic, N.; Riley, M. J.; Bortoluzzi, A. J.; Szpoganicz, B.; Schenk, G.; Neves, A.; Gahan, L. R. *J. Biol. Inorg. Chem.* **2007**, *12*, 1207–1220.
(23) Schenk, G.; Peralta, R. A.; Batista, S. C.; Bortoluzzi, A. J.; Szpoganicz, B.; Dick, A. K.; Herrald, P.; Hanson, G. R.; Szilagyi, R. K.; Riley, M. J.; Gahan, L. R.; Neves, A. *J. Biol. Inorg. Chem.* **2008**, *13*, 139–155.
(24) Beck, J. L.; McConachie, L. A.; Summors, A. C.; Arnold, W. N.; de Jersey, J.; Zerner, B. *Biochim. Biophys. Acta* **1986**, *869*, 61–68.
(25) Schenk, G.; Ge, Y.; Carrington, L. E.; Wynne, C. J.; Searle, I. R.; Carroll, B. J.; Hamilton, S. E.; de Jersey, J. *Arch. Biochem. Biophys.* **1999**, *370*, 183–189.
(26) Durmus, A.; Eicken, C.; Sift, B. H.; Kratel, A.; Kappl, R.; Hüttermann, J.; Krebs, B. *Eur. J. Biochem.* **1999**, *260*, 709.
(27) Twitchett, M. B.; Sykes, A. G. *Eur. J. Inorg. Chem.* **1999**, 2105–2115.
(28) Truong, N. T.; Naseri, J. I.; Vogel, A.; Rompel, A.; Krebs, B. *Arch. Biochem. Biophys.* **2005**, *440*, 38–45.
(29) Funhoff, E. G.; Wang, Y.; Andersson, G.; Averill, B. A. *FEBS J.* **2005**, *272*, 2968–2977.
(30) Cox, R. S.; Schenk, G.; Mitić, N.; Gahan, L. R.; Hengge, A. C. *J. Am. Chem. Soc.* **2007**, *129*, 9550–9551.
(31) Schenk, G.; Elliott, T. W.; Leung, E. W. W.; Mitić, N.; Carrington, L. E.; Gahan, L. R.; Guddat, L. W. *BMC Struct. Biol.* **2008**, *8*, 6.
(32) Schenk, G.; Boutchard, C. L.; Carrington, L. E.; Noble, C. J.; Moubaraki, B.; Murray, K. S.; de Jersey, J.; Hanson, G. R.; Hamilton, S. E. *J. Biol. Chem.* **2001**, *276*, 19084–19088.
(33) Hadler, K. S.; Tanifum, E. A.; Yip, S.; Mitić, N.; Guddat, L. W.; Jackson, C. J.; Gahan, L. R.; Nguyen, K.; Carr, P. D.; Ollis, D. L.; Hengge, A. C.; Larrabee, J. A.; Schenk, G. *J. Am. Chem. Soc.* **2008**, *130*, 14129–14138.

$$(P)_{app} = \frac{(P)_{max}}{\left(1 + \frac{[H^+]}{K_1} + \frac{K_2}{[H^+]}\right)} \quad (2)$$

where P corresponds to k_{cat} or k_{cat}/K_M and K_v ($v = 1, 2$) corresponds to K_{es} or K_e, respectively (K_e represents the protonation equilibrium associated with the free enzyme or free substrate).

Electron Paramagnetic Resonance (EPR) Spectroscopy. X-band continuous wave (CW) EPR spectra were obtained using a Bruker Biospin Elexsys E580 EPR spectrometer fitted with a super high Q cavity. The magnetic field and microwave frequency were calibrated with a Bruker ER036M Teslameter and Bruker frequency counter, respectively. Computer simulation of the EPR spectra and generation of energy level diagrams and transition road maps were carried out with Molecular Sophe (MoSophe, v2.1.2) running on a personal computer with the Mandriva 2008 operating system.[34] Optimization of the spin Hamiltonian parameters involved combining MoSophe and the optimization algorithms within Octave.[34,35]

Results and Discussion

Protein Purification and Characterization. The Mn derivative of the native spPAP, purified as described previously,[25] was incubated at RT with a chelating agent (1,10-phenanthroline) and a reductant (sodium dithionite) to first reduce Fe^{III} to Fe^{II} and then extract both divalent metal ions as 1,10-phenanthroline metal-ion complexes. The protein was separated from the 1,10-phenanthroline and its metal-ion complexes by passing it through a low-molecular-weight size-exclusion column. Subsequently, 50 equiv of $MnCl_2$ was added and the mixture allowed to stand at RT for several days until maximal kinetic activity was reached (~100 h). The excess of manganese was then removed by dialysis against 0.1 M acetate buffer, pH 4.9. The metal-ion content of the native enzyme (FeMn-spPAP) was determined to be 1.06 ± 0.08 g-atoms of Fe and 0.82 ± 0.05 g-atoms of Mn per active site, with trace amounts of Zn and Cu (<0.05 g-atoms). In contrast, the manganese derivative of spPAP (MnMn-spPAP) contained only 0.11 ± 0.02 g-atoms of Fe but nearly 2 equiv of Mn (1.93 ± 0.08 g-atoms; the Zn and Cu amounts were below the detection limits).

A comparison of the UV/vis spectra of FeMn-spPAP and MnMn-spPAP reveals a significant drop in intensity of the Tyr-to-Fe^{III} charge-transfer band at 560 nm (FeMn-spPAP:[25] λ_{max} = 560 nm, ε = 3200 $M^{-1}cm^{-1}$; MnMn-spPAP: λ_{max} = 549 nm, ε = 350 $M^{-1}cm^{-1}$). Because the metal-ion analysis indicates the presence of 0.11 g-atom of Fe (incomplete removal of the Fe^{III} center), it is likely that the band at 549 nm arises from 11% of strongly antiferromagnetically coupled (EPR-silent) Fe^{III}-(μ-O)-Mn^{II} centers in MnMn-spPAP. Longer incubations with higher concentrations of denaturant have not facilitated the complete removal of iron from the active site.

EPR Spectroscopy. EPR spectroscopy was employed to probe the electronic structure of the active site of MnMn-spPAP. The EPR spectrum reveals resonances arising from an extraneous mononuclear Mn^{II} ($S = {}^5/_2$, $I = {}^5/_2$; $g = 2$, $A/g\beta$ = ~9.3 mT) center (<5%) and Mn hyperfine resonances on either side of this feature (Figure 2). These hyperfine resonances are separated by $A/g\beta$ = 4.45 mT, which is half that expected for a

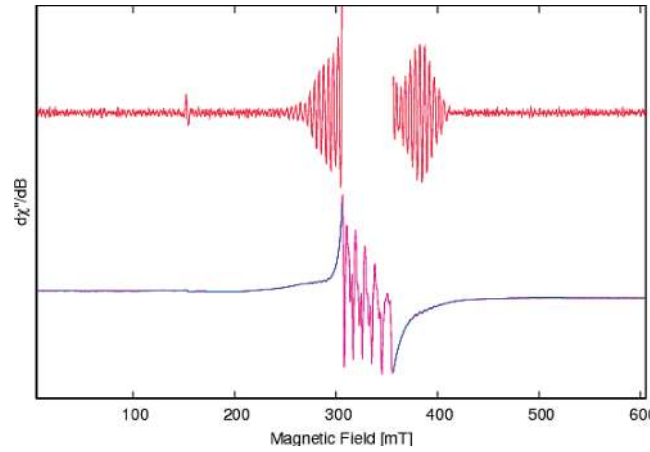

Figure 2. EPR spectra of MnMn-spPAP showing the experimental spectrum (purple), a cubic 55 point (low- and high-field sections) Savitzky−Golay[41] filter (blue) and the resultant spectral subtraction (red). The resonance at 160 mT arises from a magnetically isolated Fe^{III} center.

mononuclear Mn^{II} species, and characteristic of an exchange-coupled dinuclear Mn^{II} center.[36−40]

EPR spectra of dinuclear manganese species can be described by a total spin Hamiltonian involving the sum of the individual spin Hamiltonians for each Mn ion ($i = 1, 2$) and the interaction Hamiltonian (eq 3).[42−44]

$$\begin{aligned} H_{tot} &= H_1 + H_2 + H_{12} \\ H_i &= \mathbf{S}_i\cdot\mathbf{D}_i\cdot\mathbf{S}_i + \beta\mathbf{B}\cdot\mathbf{g}_i\cdot\mathbf{S}_i + \mathbf{S}_i\cdot\mathbf{A}_i\cdot\mathbf{I}_i + \mathbf{I}_i\cdot\mathbf{Q}_i\cdot\mathbf{I}_i - \\ &\qquad \gamma(1 - \boldsymbol{\sigma}_i)\mathbf{B}\cdot\mathbf{I}_i \quad (i = 1, 2) \\ H_{12} &= -2J\mathbf{S}_1\cdot\mathbf{S}_2 + \mathbf{G}_{12}\mathbf{S}_1 \times \mathbf{S}_2 + \mathbf{S}_1\cdot\mathbf{D}_{12}\cdot\mathbf{S}_2 \end{aligned} \quad (3)$$

where **S** and **I** are the electron and nuclear spin operators, respectively, **D** is the zero-field splitting tensor, **g** and **A** are the electron Zeeman and hyperfine coupling matrices, respectively, **Q** is the quadrupole tensor, γ is the nuclear gyromagnetic ratio, ´$\boldsymbol{\sigma}$ is the chemical shift tensor, β is the Bohr magneton, and B is the applied magnetic field. The interaction Hamiltonian (H_{12}, eq 3) accounts for the isotropic ($H_{ex} = -2J\ \mathbf{S}_1\cdot\mathbf{S}_2$), antisymmetric ($H_{as} = \mathbf{G}_{12}\ \mathbf{S}_1 \times \mathbf{S}_2$) and anisotropic exchange (dipole−dipole coupling, $H_{dd} = \mathbf{S}_1\cdot\mathbf{D}_{12}\cdot\mathbf{S}_2$) interactions between the two manganese centers.

In the strong exchange limit ($|2J| > |D|$) the spin system is best characterized by a total spin operator, $\mathbf{S}_T = \mathbf{S}_1 + \mathbf{S}_2$; for two antiferromagnetically coupled high-spin Mn^{II} ($S = {}^5/_2$) ions, there are a total of six spin multiplets characterized by $S_T = 0$, 1, 2, 3, 4, and 5, where $S_T = 0$ is the ground spin state and

(34) Hanson, G. R.; Noble, C. J.; Benson, S. *Biol. Magn. Reson.* **2009**, *28*, 105–174.
(35) Octave is open source software and can be downloaded from http://www.gnu.org/software/octave/.
(36) Khangulov, S. V.; Pessiki, P. J.; Barynin, V. V.; Ash, D. E.; Dismukes, G. C. *Biochemistry* **1995**, *34*, 2015–2025.
(37) Rusnak, F.; Yu, L.; Todorovic, S.; Mertz, P. *Biochemistry* **1999**, *38*, 6943–6952.
(38) Howard, T.; Telser, J.; de Rose, V. J. *Inorg. Chem.* **2000**, *39*, 3379–3385.
(39) Golombek, A. P.; Hendrich, M. P. *J. Magn. Reson.* **2003**, *165*, 33–48.
(40) Epel, B.; Schäfer, K.-O.; Quentmeier, A.; Friedrich, C.; Lubitz, W. *J. Biol. Inorg. Chem.* **2005**, *10*, 636–642.
(41) Savitzky, A.; Golay, M. A. *J. Anal. Chem.* **1964**, *36*, 1627–1639.
(42) Pilbrow, J. R. *Transition Ion Electron Paramagnetic Resonance*; Oxford University Press: Oxford, 1990.
(43) Smith, T. D.; Pilbrow, J. R. *Coord. Chem. Rev.* **1974**, *13*, 173–278.
(44) Bencini, A.; Gateschi, D. *EPR of Exchange Coupled Systems*; Springer-Verlag: Heidelberg, 1990; p 48.

Table 1. Values of the Electron Spin (S) and Numerical Coefficients (c_1,c_2) for Various Dinuclear Mn Centers[44]

center	S_1	S_2	c_1	c_2
$Mn^{II}Mn^{II}$	$^5/_2$	$^5/_2$	$^1/_2$	$^1/_2$
$Mn^{II}Mn^{III}$	$^5/_2$	2	$^7/_3$	$-^4/_3$
$Mn^{III}Mn^{III}$	2	2	$^1/_2$	$^1/_2$
$Mn^{III}Mn^{IV}$	2	$^3/_2$	2	-1

Table 2. Numerical Coefficients (d_1, d_2, d_{12}) of the Projection Operators Given in eq 6 for Mn^{II} and Mn^{III} Dimers[44]

S_1	S_2	S_T	d_1	d_2	d_{12}
$^5/_2$	$^5/_2$	1	$-^{16}/_5$	$-^{16}/_5$	$+^{37}/_{10}$
		2	$-^{10}/_{21}$	$-^{10}/_{21}$	$+^{41}/_{42}$
		3	$-^1/_{45}$	$-^1/_{45}$	$+^{47}/_{90}$
		4	$+^1/_7$	$+^1/_7$	$+^5/_{14}$
		5	$+^2/_9$	$+^2/_9$	$+^5/_{18}$
2	2	1	$-^{21}/_{10}$	$-^{21}/_{10}$	$+^{13}/_5$
		2	$-^3/_{14}$	$-^3/_{14}$	$+^5/_7$
		3	$+^1/_{10}$	$+^1/_{10}$	$+^2/_5$
		4	$+^3/_{14}$	$+^3/_{14}$	$+^2/_7$

each of the spin multiplets is $(2S_T + 1)$-fold degenerate. The energies of these levels are given by[44]

$$E(S_T) = -J[S_T(S_T + 1) - S_1(S_1 + 1) - S_2(S_2 + 1)] \quad (4)$$

and the energy level difference between adjacent levels is

$$E(S_T) - E(S_T - 1) = -2S_TJ \quad (5)$$

For a strongly antiferromagnetically exchange coupled dinuclear Mn^{II} center only the ground spin state ($S_T = 0$) will be populated and the system is EPR-silent. A strong exchange interaction is mediated by a μ-O bridge (note that in the isolelectronic Fe^{III}-μ-O-Mn^{II} center of FeMn-spPAP $|-2J| > 140$ cm^{-1}).[32] Protonation of the μ-oxo bridging ligand (μ-OH or μ-OH_2) reduces the magnitude of the exchange coupling, resulting in either (i) complex EPR spectra if $|-2J|$ is of a similar order of magnitude as |D|, or (ii) EPR spectra that arise only from transitions within the S_T spin states, providing $|-2J|$ is greater than the microwave quantum ($h\nu$), as is usually the case at X-band frequencies. A variable temperature study from 2 to 200 K showed that the resonances centered at 298.4 and 383.7 mT initially increased, and then gradually decreased, consistent with an antiferromagnetically coupled dinuclear Mn center in the MnMn−spPAP enzyme. Consequently, the various spin Hamiltonian interactions for each individual ion in eq 3 can be simplified by treating them as a perturbation of the isotropic exchange interaction, enabling the overall manganese hyperfine and zero-field splittings to be written as[44]

$$H_S = \beta\mathbf{B}\cdot\mathbf{g}_s\cdot\mathbf{S}_T + \mathbf{S}_T\cdot\mathbf{D}_S\cdot\mathbf{S}_T + c_1\mathbf{S}_T\cdot\mathbf{A}_1\cdot\mathbf{I}_1 + c_2\mathbf{S}_T\cdot\mathbf{A}_2\cdot\mathbf{I}_2$$

$$\mathbf{g}_s = c_1\mathbf{g}_1 + c_2\mathbf{g}_2$$
$$\mathbf{D}_s = d_1\mathbf{D}_1 + d_2\mathbf{D}_2 + d_{12}\mathbf{D}_{12} \quad (6)$$

where the values of c_i, d_i, and d_{ij} ($i, j = 1, 2$; $i \neq j$) are the numerical coefficients of the projection operators and depend upon the values of S_i and the resultant S_T (Tables 1 and 2).

For dinuclear Mn^{II} and Mn^{III} $c_1 = c_2 = 0.5$ and consequently the intensity ratio of the 11 equally spaced manganese hyperfine resonances ($A_{eff} = {}^1/_2(A/g\beta)$) in the EPR spectrum

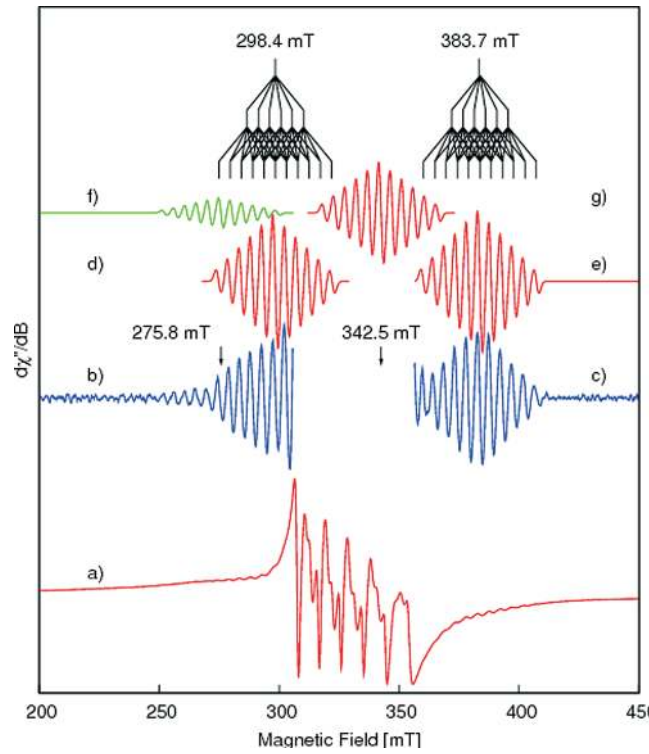

Figure 3. EPR spectrum of MnMn-spPAP at pH 6.5. $\nu = 9.382041$ GHz, $T = 4.7$ K. The insets show an expansion of the experimental (b,c) resonances associated with the dinuclear Mn^{II} center after baseline correction with a cubic 55-point (low- and high-field sections) Savitzky−Golay filter.[41] (d,e) Computer simulation of (b) and (c), respectively, with the parameters $g_S = 2.0023$, $A_1 = A_2 = 44.5 \times 10^{-4}$ cm^{-1}, $D_S = 410 \times 10^{-4}$ cm^{-1}. (f,g) Fitting of the 11 line multiplets at 275.8 and 342.5 mT, respectively.

of MnMn-spPAP would be expected to be 1:2:3:4:5:6:5:4:3:2:1. Because resonances from the mononuclear Mn^{II} center overlap with these resonances in the spectrum (Figures 2 and 3) and are themselves inhomogeneously broadened by a distribution of D and E values, we have fitted a cubic Savitzky−Golay filter[41] based on 55 points for the low- and high-field regions (Figures 2 and 3) to establish the relative intensities of the manganese hyperfine resonances and they do indeed have the expected ratio (Figure 3).

This intensity ratio of 1:2:3:4:5:6:5:4:3:2:1 effectively rules out a mixed-valent dinuclear Mn center (Table 1) as the numerical coefficients (c_i) of the projection operators would not yield 11 equally spaced multiline resonances with this intensity ratio. Thus, these resonances arise from either a dinuclear Mn^{II} or Mn^{III} center. Interestingly, the only resonances observed in the EPR spectrum of MnMn-spPAP are those centered at 275.8, 298.4, 342.5, and 383.7 mT (Figure 3). This can be readily explained by the presence of a large distribution of zero-field splitting parameters. Replacement of D_s, D_1, D_2, and D_{12} by ΔD_s, ΔD_1, ΔD_2, and ΔD_{12} in eq 6 and a comparison of the numerical coefficients (d_1, d_2, and d_{12}, Table 2) of the projection operators shows that transitions only from an $S_T = 3$ spin state of a dinuclear Mn^{II} center would be observed (smallest values of d_1 and d_2) as all of the resonances from other spin states ($Mn^{II}Mn^{II}$: $S_T = 1, 2, 4, 5$; $Mn^{III}Mn^{III}$: $S_T = 1, 2, 4$) would exhibit

(45) EPR spectra of dinuclear manganese model complexes have been shown to arise from an $S_T = 2$ spin state, although additional transitions to those observed here were found, indicating that the zero-field splitting and/or the distribution of zero-field splitting parameters was much smaller.

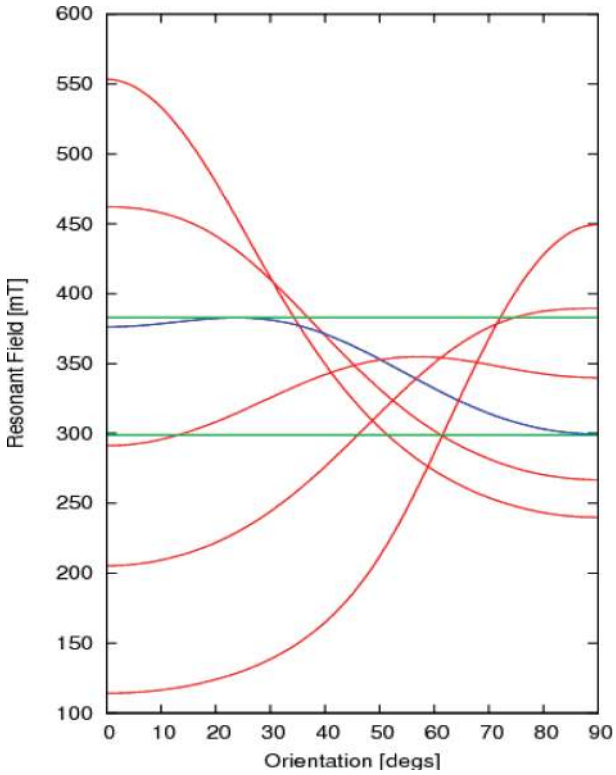

Figure 4. Transition road map showing orientational dependence of the resonant field positions (red, blue) of each of the transitions within the $S_T = 3$ spin state with respect to the external magnetic field. The blue curve corresponds to the $\Delta M_S = -1 \leftrightarrow 0$ transition. The green lines correspond to the centers of the 11 line multiplets at 298.4 and 383.7 mT.

significant strain broadening.[45] In addition, the magnitude of $A/g\beta$ (44.5 mT) and the loss of acidic phosphatase activity (vide infra) are consistent with a dinuclear Mn^{II} center in MnMn-spPAP.

To gain insight into the origin of the resonances, we employed Molecular Sophe[34] (MoSophe) and Octave[35] to simulate (fit) each of the four 11 line multiplets (Figure 3) with an effective spin Hamiltonian (eq 7) with $S_{eff} = {}^1/_2$

$$H_{eff} = \beta g_{iso}\mathbf{B}\cdot\mathbf{S_{eff}} + \mathbf{S_{eff}}\cdot\mathbf{A}_1\cdot\mathbf{I}_1 + \mathbf{S_{eff}}\cdot\mathbf{A}_2\cdot\mathbf{I}_2 \qquad (7)$$

to determine the resonant field positions for each of the multiplets and the hyperfine couplings. Once the resonant field positions were determined (Figure 3), we undertook computer simulations (spectra, energy level diagrams, and road maps) using MoSophe[34] and the spin Hamiltonian in eq 6 to fit the resonant field positions, assuming the resonances arise from an $S_T = 3$ spin state. The following spin Hamiltonian parameters ($g_s = 2.0023$, $A_1 = A_2 = 44.5 \times 10^{-4}$ cm^{-1}, $D_S = 410 \times 10^{-4}$ cm^{-1}) were found to reproduce the resonant field positions at 298.4 and 383.7 mT (Figure 3).

An inspection of Figure 4 shows that the resonances arise from the $\Delta M_S = -1 \leftrightarrow 0$ transition (blue) and that the low-field resonances centered at 298.4 mT (Figure 3) correspond to perpendicular resonances (extremum at 90°, Figure 4) and those at 383.7 mT (Figure 3) correspond to an off-axis extremum at ~20° (Figure 4). Introducing a distribution of zero-field splittings (E-strain) results in broadening of the resonances arising

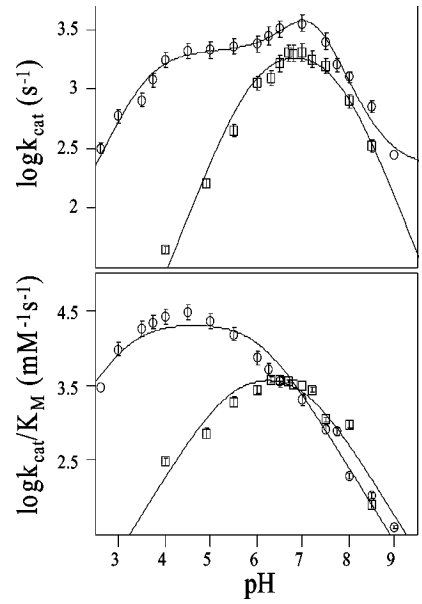

Figure 5. pH dependence of the kinetic parameters of native FeMn-spPAP (circles) and MnMn-spPAP (squares). The data points are determined experimentally and the solid lines represent fits to the data using eqs 1 and 2 and procedures described elsewhere.[22,33]

from all of the transitions shown in red in Figure 4. Close examination of the experimental spectrum with the baseline subtracted (Figure 3) reveals additional resonances (not readily apparent) in the experimental spectrum centered at 342.5 and 275.8 mT. The former corresponds to perpendicular resonances of the $\Delta M_S = 0 \leftrightarrow 1$ transition whereas the origin of the latter resonances is at this stage unknown, although they may arise through state mixing (intermediate exchange regime) if J were relatively small (~2 cm^{-1}) but still larger than D_1 and D_2 ~ 0.1 cm^{-1} and $h\nu$.

Examination of the numerical coefficients d_1, d_2, and d_{12} for the $S_T = 3$ spin state (Table 2) reveals that the zero-field splittings for each individual Mn^{II} center will contribute negligibly to D_S and furthermore that the major contribution to D_S arises from the dipole−dipole interaction. D_{12} is therefore estimated to be 745×10^{-4} cm^{-1} using the given value of d_{12}. Using the point dipole−dipole approximation and assuming an isotropic g factor (eq 8) yield an internuclear distance of 4.05 Å.

$$D_{12} = \frac{3g^2\beta^2\mu_0}{4\pi r^3} \qquad (8)$$

This represents an upper limit for the internuclear distance as the values of D_1 and D_2 will be nonzero, and without additional spectroscopic information their contribution cannot be defined as their magnitude, orientation of their principal axes, and sign remain unknown. A comparison of the internuclear Mn−Mn distance with the type of bridging ligand (μ-O, μ-OH, μ-OH_2, and μ-CH_3CO_2) for some representative model complexes $[Mn_2(\mu\text{-}O)_2(H_2O)_8]$ (r(Mn−Mn) = 2.890 Å),[47,48] $Mn_2[Ru(CN)_8]\cdot 8H_2O$ ([Mn-(μ-OH_2)$_2$-Mn], r(Mn−Mn) = 3.7

(46) Zhang, L.; Crossley, M. J.; Dixon, N. E.; Ellis, P.; Fisher, M. L.; King, G. L.; Lilley, P. E.; MacLachlan, D.; Pace, R. J. *J. Biol. Inorg. Chem.* **1998**, *3*, 470–483.

(47) Mitani, M.; Wakamatsu, Y.; Katsurada, T.; Yoshioka, Y. *J. Phys. Chem. A* **2006**, *110*, 13895–13914.

(48) Liu, S. B.; Perera, L.; Pedersen, L. G. *Mol. Phys.* **2007**, *105*, 2893–2898.

Table 3. Catalytic Parameters for the Hydrolysis of *p*-NPP for FeMn- and MnMn-spPAP[a]

enzyme	$k_{cat,max}$ (s^{-1})	$(k_{cat}/K_M)_{max}$ (s^{-1} mM^{-1})	pK_{e1}	pK_{e2}	pK_{es1}	pK_{es2}	pK_{es3}
FeMn-spPAP	12700 ± 960	21390 ± 4150	3.20 ± 0.15	6.10 ± 0.10	3.70 ± 0.20	6.90 ± 0.15	7.60 ± 0.15
MnMn-spPAP	5500 ± 700	4705 ± 775	5.40 ± 0.20	7.10 ± 0.20	6.80 ± 0.20		7.40 ± 0.15

[a] The pH dependence of k_{cat} for FeMn-spPAP indicates that at least three protonation equilibria are relevant to catalysis. k_{cat1} corresponds to the fully protonated form of the enzyme and k_{cat4} to the fully deprotonated form. The fitted parameters are as follows: $k_{cat1} = 160 \pm 80$ s^{-1}; $k_{cat2} = 2270 \pm 100$ s^{-1}; $k_{cat3} = k_{cat,max}$ 12700 ± 960 s^{-1}; $k_{cat4} \sim 0$.

Å),[49] $[L'_2Mn_2(\mu\text{-}OH)(\mu\text{-}CH_3CO_2)_2](ClO_4)$ (r(Mn−Mn) = 3.5 ± 0.2 Å),[50] $[L'_2Mn_2(\mu\text{-}CH_3CO_2)_3](BPh_4)$ (r(Mn−Mn) = 4.034 Å),[50] and $[Mn_2(\mu\text{-}OH)L]^{3+}$ (r(Mn−Mn) = 3.615 Å)[51] and enzymes such as FeMn-spPAP ([Fe^{III}-μ(O)-Mn^{II}] (r(Mn−Mn) = 3.26 Å),[13e] catalase ([Mn-(μ-OH_2)(μ-CH_3CO_2)$_{1-2}$-Mn], r(Mn−Mn)= 3.59 Å),[36] and the multiple forms of arginase (r(Mn−Mn) = 3.36−3.57 Å)[36,52] indicates that a μ-O bridging ligand is not present in the active site of MnMn-spPAP and that most likely the bridging ligands consist of one or more μ-OH, μ-OH_2, and μ-RCO_2 functional groups.

Catalytic Parameters and Mechanism of MnMn-spPAP. We further examined the kinetic competency of this $Mn^{II}Mn^{II}$-spPAP and demonstrate that the enzyme no longer functions as an acid phosphatase but is fully active as a functional pH neutral phosphatase. The pH dependence of the k_{cat} and k_{cat}/K_M values for both FeMn-spPAP and MnMn-spPAP is shown in Figure 5.

The pH dependence of k_{cat} of the native enzyme displays unusual behavior with a broad shoulder at low pH and a maximum at neutral pH. The data were fit to an equation (eq 1) derived for a model invoking three protonation equilibria (pK_{es1}−pK_{es3}).[22,33] The corresponding parameters are listed in Table 3. For the MnMn-spPAP enzyme only two protonation equilibria (pK_{es1} and pK_{es3}) are required to account for the observed pH dependence of k_{cat} (eq 2), but the optimum is at a similar pH (Figure 5). In contrast, the relative pH optima for FeMn- and MnMn-spPAP differ significantly for the k_{cat}/K_M ratio with pH 4.5 and pH 6.5, respectively. Both data sets display bell-shape behavior, requiring two protonation equilibria (pK_{e1} and pK_{e2}; Table 3).[22,53]

In essence, upon replacing the Fe^{III} by Mn^{II}, spPAP loses significantly its ability to act as an acid phosphatase. In the accepted mechanistic models for PAP-catalyzed reactions the chromophoric metal ion activates the nucleophile.[13b,e,14,29,31,54−56] Thus, the shift of the catalytic efficiency (k_{cat}/K_M) of MnMn-spPAP toward a significantly more alkaline pH is in agreement with the oxidation state of the manganese in the chromophoric site being divalent. On the basis of the metal-ion analysis and optical spectrum, it is anticipated that up to 10% of the activity of MnMn-spPAP is due to the presence of FeMn centers (vide supra). This may account for the minor deviations from bell-shaped behavior observed in the pH profile of k_{cat} (Figure 5, top). Assuming a 10% contamination of the MnMn-spPAP sample with FeMn centers, the activity of the dimanganese derivative at pH 7.0 (close to the pH maximum; Figure 5) can be estimated to be 1875 s^{-1}, approximately half the value determined for the native enzyme (3550 s^{-1}).[13e]

Table 4. Tentative Assignments of pK_a Values to Relevant Deprotonations in the Active Site of spPAP

pK_a	FeMn-spPAP	MnMn-spPAP
pK_{e1}	Glu_{365}-COOH	*p*-NPPH
pK_{e2}	*p*-NPPH	His_{295}-NH
pK_{es1}	μ-OH^-	μ-H_2O
pK_{es2}	His_{201}-NH	
pK_{es3}	His_{295}-NH	His_{295}-NH

Although the assignment of pK_a values to corresponding protonation equilibria in enzymes is difficult, the comparison of these values for two metal-ion derivatives of the same enzyme provides insight into the catalytically relevant functional groups. Table 4 summarizes tentative assignments. pK_{es3} (and pK_{e2} for MnMn-spPAP) is likely to be associated with the conserved His295 because replacement of the only other conserved histidine residue in the PAP substrate binding pocket (His201) did not result in the loss of the alkaline limb in the pH profile.[28,29]

Together with His201 and Glu365, a residue that is not conserved among PAPs, His295 is expected to be involved in substrate and/or nucleophile positioning in spPAP (Figure 1).[13e] These three residues are involved in extensive H-bond interactions in the second coordination sphere, and their protonation states are expected to affect both substrate binding and reactivity. The dramatic change in the catalytic properties of the enzyme upon replacing the chromophoric Fe by Mn suggests that the mode of substrate binding is also altered. The pK_{a2} for *p*-NPP is ∼5.5. Thus, pK_a values in the range 5.5−6.0 (pK_{e2} and pK_{e1} for FeMn- and MnMn-spPAP, respectively; Table 4) are likely to correspond to the substrate, suggesting that *p*-NPP binds preferentially in its monoanionic form to FeMn-spPAP, but in its dianionic form to the Mn derivative. The remaining pK_a values (pK_{es1}) are ascribed to the nucleophiles. The native enzyme (FeMn-spPAP) is likely to have a μ-oxo group at pH 4.9 based on the observation of very strong antiferromagnetic coupling at this pH.[32] In contrast, pK_{es1} in the MnMn-spPAP enzyme is alkaline-shifted by ∼3 units (Table 3). This value is too low to be assigned to a water molecule bound terminally to

(49) Rüegg, M.; Ludi, A.; Reider, K. *Inorg. Chem.* **1970**, *10*, 1773–1777.
(50) Wieghardt, K.; Bossek, U.; Nuber, B.; Weiss, J.; Bonvoisin, J.; Corbella, M.; Vitols, S. E.; Girerd, J. J. *J. Am. Chem. Soc.* **1998**, *110*, 7398–7411.
(51) Tétard, D.; Rabion, A.; Verlhac, J.-B.; Guilhem, J. *J. Chem. Soc., Chem. Commun.* **1995**, 531–532.
(52) Cama, E.; Pethe, S.; Boucher, J.-L.; Han, S.; Emig, F. A.; Ash, D. E.; Viola, R. E.; Mansuy, D.; Christianson, D. W. *Biochemistry* **2004**, *43*, 8987–8999.
(53) (a) Cleland, W. W. *Adv. Enzymol. Relat. Areas Mol. Biol.* **1977**, *45*, 273–387. (b) Cleland, W. W. *Adv. Enzymol. Relat. Areas Mol. Biol.* **1967**, *29*, 1–32. (c) Cleland, W. W. *Annu. Rev. Biochem.* **1967**, *36*, 77–112.
(54) Mitić, N.; Valizadeh, M.; Leung, E. W. W.; de Jersey, J.; Hamilton, S.; Hume, D. A.; Cassady, A. I.; Schenk, G. *Arch. Biochem. Biophys.* **2005**, *439*, 154–164.
(55) Merkx, M.; Pinkse, M. W. H.; Averill, B. A. *Biochemistry* **1999**, *38*, 9914–9925.
(56) Smoukov, S. K.; Quaroni, L.; Wang, X. D.; Doan, P. E.; Hoffman, B. M.; Que, L., Jr. *J. Am. Chem. Soc.* **2002**, *124*, 2595–2603.
(57) Samples, C. R.; Howard, T.; Raushel, F. M.; DeRose, V. J. *Biochemistry* **2005**, *44*, 11005–11013.

a Mn^{II}, but is in a region expected for water molecules that are doubly Lewis-activated by divalent metal ions.[57]

Conclusions

Herein, we have presented a new methodology for the analysis of EPR spectra from dinuclear Mn^{II} centers which, when combined with the kinetic data, indicate the presence of an antiferromagnetically coupled Mn^{II}-μ-(H)OH-μ-carboxylato-Mn^{II} center in spPAP (Figure 1), the first homodivalent, catalytically active form of a PAP. The replacement of the Fe^{III} by Mn^{II} converts the acid phosphatase into a phosphatase that operates optimally under neutral pH conditions. It thus appears that PAP may have evolved from homodivalent ancestors in response to its biological function in often acidic environments (e.g., bone resorptive space and soil[8]). Furthermore, the results presented in this study demonstrate the importance of having a trivalent metal ion for acid phosphatase activity, thus increasing our understanding of the role of the chromophoric metal ion as an activator of the nucleophile in acid hydrolysis. The detailed analysis of strain broadened EPR spectra of antiferromagnetically coupled dinuclear Mn^{II} centers allows the oxidation states of the manganese ions and the internuclear distance to be determined. The new EPR methodology presented herein will also be useful for the analysis of EPR spectra from other dinuclear Mn metalloenzymes, for example, the 3′-5′ exonuclease DNA proofreading activity from *Escherichia coli* (Figure S1, Supporting Information),[58] the glycerophophodiesterase GpdQ from *Enterobacter aerogenase*,[33] and the manganese transport regulator protein from *Bacillus subtilis*.[59]

Acknowledgment. We thank the Australian Research Council and Bruker Biospin for financial support and Kieran Hadler for preparation of Figure 1.

Supporting Information Available: An EPR spectrum of the dimanganese^{II} exonuclease is provided. This material is available free of charge via the Internet at http://pubs.acs.org.

JA900797U

(58) Hamdan, S.; Bulloch, E. M.; Thompson, P. R.; Beck, J. L.; Yang, J. Y.; Crowther, J. A.; Lilley, P. E.; Carr, P. D.; Ollis, D. L.; Brown, S. E.; Dixon, N. E. *Biochemistry* **2002**, *41*, 5266–5275.

(59) Golyynski, M.; Gunderson, W. A.; Hendrich, M. P.; Cohen, S. M. *Biochemistry* **2006**, *45*, 15359–15372.